Asynchronous Vibration Response Characteristics of Aero-Engine With Support Looseness Fault

H. F. Wang[1]
College of Civil Aviation,
Nanjing University of Aeronautics
and Astronautics,
No. 29, Jiangjun Dadao, Jiangning District,
Nanjing 211106, China
e-mail: wanghaifei1986318@163.com

G. Chen
College of Civil Aviation,
Nanjing University of Aeronautics
and Astronautics,
No. 29, Jiangjun Dadao, Jiangning District,
Nanjing 211106, China
e-mail: cgzyx@263.net

P. P. Song
College of Civil Aviation,
Nanjing University of Aeronautics
and Astronautics,
No. 29, Jiangjun Dadao, Jiangning District,
Nanjing 211106, China
e-mail: spp0104@sina.com

In this paper, the mechanism of the asynchronous vibration response phenomenon caused by the looseness fault in the aero-engine whole vibration system is investigated by numerical integration methods. A single degree-of-freedom (DOF) lumped mass model and a rotor-casing whole vibration model of a real engine are established, and two looseness fault models are introduced. The response of these two systems is obtained by numerical integration methods, and the asynchronous response characteristics are analyzed. By comparing the response of a single DOF lumped mass model with the response of multiple DOF model, the reason leading to the asynchronous response characteristics is the relationship between the changing period of stiffness and the changing period of the rotational speed. When the changing period of stiffness is equivalent to the changing period of the rotational speed, frequency multiplication will appear and the natural frequency will be excited at specific speeds. When the changing period of stiffness is equivalent to n (n = 2, 3,…) times the changing period of the rotating speed, 1/n (n = 2, 3,…) frequency division and frequency multiplication will appear and the natural frequency will be excited at specific speeds. [DOI: 10.1115/1.4031245]

Keywords: asynchronous response characteristics, looseness fault, looseness characteristics, dynamical model, whole vibration modeling

1 Introduction

Due to the low bearing stiffness in aero-engine, the wide use of thin-walled structure in rotor and casing, its great flexibility, looseness phenomenon is universal. An unforeseen array of asynchronous response frequencies at other than the critical was noted when the aero-engine was operated at both subcritical and supercritical speeds. However, those responses were not explored in detail at the time. To understand the essence of looseness fault better, the analysis of asynchronous response characteristics is of great significance.

Many scholars have studied the looseness fault based on lumped mass model. Ehrich [1] used a simple numerical model of a rotor employing a piecewise linear (that is, a bilinear) bearing support stiffness to represent the system, it was possible to replicate the new class of asynchronous rotor dynamic response in high-speed rotors over a range of sub-, trans-, and supercritical high-speed rotor operation. Muszynska et al. [2] established a rotor-bearing-stator model with a one-lateral-mode unbalanced, bearing looseness, and rotor–stator rubbing, showing the nonlinear characteristics of the periodic vibrations of synchronous (1×), subsynchronous (1/2×, 1/3×…), and multiples (2×, 3×…). Yushu and Shihai [3] adopted a new method to study the sub/superharmonic resonance of nonlinear system with single DOF and subharmonic solution of a piecewise linear oscillator with two DOF. Chu and Tang [4] investigated the vibration characteristics of a rotor-bearing system with pedestal looseness, used the shooting method to obtain the periodic solutions, and analyzed the steady of the periodic solutions by the Floquet theory. Guo [5] established an unbalance-rubbing coupling faults dynamic model with rolling bearing-rotor system and obtained the nonlinear dynamic response laws of rotor-ball bearing-stator system under unbalance and rubbing coupling fault. Goldman and Muszynska [6] developed an analytical algorithm for investigating local nonlinear effects in rotor systems. They used a specially developed variable transformation that smoothes discontinuities, and then they applied an averaging technique. Their results showed good agreement with experimentally observed typical behaviors and orbits of rubbing rotors. In the last two papers, the effects of pedestal looseness on the system response were also studied. Lu and Chu [7] studied the looseness fault of rotor system by experiments. The characteristics of multiple frequency and frequency division were found. Ji and Zu [8] analyzed the free and forced vibration of a nonlinear bearing system to illustrate the nonlinear effect on the free and forced vibrations of the system by the method of multiple scales. Method multiple scales were used to study the superharmonic resonance and the subharmonic resonance [9,10]. Lu et al. [11] analyzed the stability of reduced rotor pedestal looseness fault model. In all the previous studies, experiments, nonlinear dynamics analysis, and characteristics analysis based on lumped mass model with looseness fault are performed gradually. However, the asynchronous response phenomenon has not been discussed fully and the results of the lumped mass model are different from that of the real aero-engine model.

In recent years, the finite element method has been used to establish looseness fault model by many scholars. Ma et al. [12] studied the nonlinear vibration characteristics of a rotor system with pedestal looseness fault under different loading conditions. Behzad and Asayeshthe [13] proposed a finite element method for studying the effects of loose rotating disks on the rotor-bearing systems' response. Ma et al. [14] established a finite element model of a rotor system with pedestal looseness stemming from a loosened bolt, and the effects of the looseness parameters on its dynamic characteristics were analyzed. Wang and Chen [15] established a rotor-support-casing whole model with looseness

[1]Corresponding author.

Contributed by the Design Engineering Division of ASME for publication in the Journal of Computational and Nonlinear Dynamics. Manuscript received April 13, 2015; final manuscript received August 3, 2015; published online October 23, 2015. Assoc. Editor: Stefano Lenci.

fault for certain type turbofan aero-engine. The casing acceleration response characteristics were analyzed. However, the asynchronous response characteristics were not studied deeply.

At present, many models with looseness fault are based on lumped mass model and finite element model without regard to the structure of real aero-engine. Many works cannot give bright and new explanation about the mechanism of the pseudocritical subharmonic resonance and the pseudocritical ultraharmonic resonance caused by the looseness fault. In this paper, lumped mass model and the finite element model with looseness fault are established, and the asynchronous vibration response characteristics are discussed by numerical integration methods.

2 A Single DOF Lumped Mass Model With Looseness Fault

2.1 A Single Disk-Rotor Model. The differential equations of the unbalance response of a single disk mounted on a massless shaft can be described as follows:

$$\begin{cases} m\ddot{u} + c\dot{u} + ku = me\omega^2 \cos \omega t \\ m\ddot{v} + c\dot{v} + kv = me\omega^2 \sin \omega t \end{cases} \tag{1}$$

where u and v are the radial displacements of the rotor, m is the mass of the disk, c is the viscous damping, k is the transverse stiffness of the shaft, e is eccentricity, and ω is rotational speed of the rotor.

2.2 A Foundation Looseness Model. In order to study the mechanism of the looseness fault between the component and the foundation, a simple mass-spring model is established, the looseness fault between the component and foundation is considered, and the mass block is always connected with the foundation, as shown in Fig. 1.

It is assumed that the mass of mass block is m, the contact stiffness between the mass block and the foundation is k_2, the damping is c, the contact stiffness between the mass block and the hard spring is k_1, the looseness clearance is δ, the vibration displacement of the mass block is x_1, and the vibration displacement of the foundation is x_2.

The differential equation of the mass block under the foundation vibration can be described as follows:

$$\begin{cases} m\ddot{x}_1 + c(\dot{x}_1 - \dot{x}_2) + k_2(x_1 - x_2) = 0 (x_1 - x_2 \le \delta) \\ m\ddot{x}_1 + c(\dot{x}_1 - \dot{x}_2) + k_2(x_1 - x_2) + k_1(x_1 - x_2 - \delta) = 0 (x_1 - x_2 > \delta) \end{cases} \tag{2}$$

It is assumed that vibration frequency of the foundation is f, the amplitude is A, so that the vibration displacement of the foundation $x_2 = A \sin(2\pi ft)$; the relative displacement between the mass block and the foundation $x = x_1$-x_2; when the looseness clearance is smaller, the relative motion equation can be described as follows:

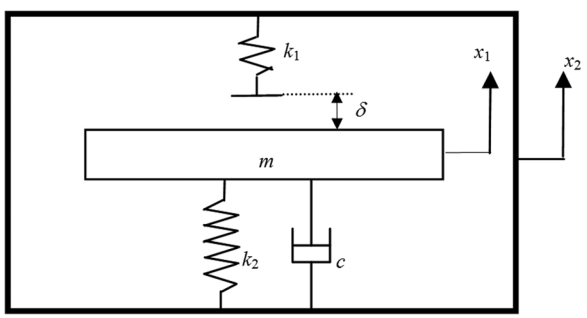

Fig. 1 Mass and foundation looseness model sketch

$$m\ddot{x} + c\dot{x} + kx = m\ddot{x}_2 \tag{3}$$

Since the second formula of Eq. (1) is similar to Eq. (3), and the looseness fault has directivity, which means the vibration in u direction and in v direction are separable, Eq. (3) can be used to simulate the single disk-rotor model with looseness fault. The relative displacement x can be used to simulate the displacement of rotor, and the relative acceleration $\ddot{x}$ can be used to simulate the acceleration of rotor.

Then, the natural frequency of the hard spring $f_1 = (k_2/m)^{1/2}$ and the natural frequency of the soft spring $f_2 = (k_1/m)^{1/2}$. It is assumed that the natural frequency of the system is f_n; the clearance δ is smaller, the vibration time is very short, and it can be ignored, so that the vibration period of this system is half of the sum of the vibration period of the hard spring and the soft spring, it can be described as follows:

$$\frac{1}{f_n} = \frac{1}{2}\left(\frac{1}{f_1}\right) + \frac{1}{2}\left(\frac{1}{f_2}\right) \tag{4}$$

2.3 Simulation Analysis of Looseness Fault. For studying the strong nonlinear characteristics caused by the looseness fault, smaller damping and larger stiffness are adopted. It is assumed that the mass of the mass block $m = 10$ kg, the vibration amplitude of the foundation $A = 100\ \mu$m, the damping between the mass block and the foundation $c = 20$ N s/m, the contact stiffness $k_2 = 9.85 \times 10^5$ N/m, and the contact stiffness k_1 between the mass block and the hard spring is $100k_2$. The natural frequency of this system, according to Eq. (4), $f_n = 90.9$ Hz.

Since numerical calculation methods are the effective way to solve strong nonlinear differential equation, the response of this system can be solved by the improved Newmark-β algorithm [16]. When the hard spring is contacted, the contact condition is marked 1, and when the soft spring is contacted, the contact condition is marked 0.

The results are shown in Figs. 2 and 3, when the vibration frequencies are $1/2f_n$ and $1/3f_n$, respectively. In Fig. 2(*a*), the waveform of relative displacement has two bounces and two peaks per revolution. Figure 2(*b*) is from literature [1] and the nondimensional method was used in the parameter y. In Fig. 2(*c*), the rotational frequency and the larger double frequency appear in the spectrum of the relative displacement. In Figs. 2(*d*) and 2(*f*), the acceleration and the relative acceleration of the mass block have two bounces per rotation. In Fig. 2(*e*), the changing period of stiffness is equivalent to the period of the rotational speed, so that frequency multiplication appears.

In Fig. 3(*a*), the waveform of the relative displacement has three bounces and three peaks per revolution. Figure 3(*b*) is from literature [1]. In Fig. 3(*c*), the rotational frequency, the larger double frequency, and the natural frequency of the system appear in the spectrum of the relative displacement. In Figs. 3(*d*) and 3(*f*), the acceleration and the relative acceleration of the mass block have three bounces per rotation. In Fig. 3(*e*), the changing period of stiffness is equivalent to the period of the rotational speed, so that frequency multiplication appears.

As can be seen from Fig. 2 to 3, when the damping is not large enough and the rotational frequency is equal to $1/J$ ($J = 1, 2\ldots$), the natural frequency of system f_n, that is, the changing period of stiffness is equal to the period of the rotational speed, superharmonic resonance will appear, which is the rotational frequency, its harmonic frequencies, and natural frequency. Method of multiple scales was used to obtain the same results [9,10]; however, the relationship between the changing period of stiffness and the changing period of the rotational speed was not investigated.

The results are shown in Figs. 4–6 when the rotational frequencies are $2/5f_n$, $3/7f_n$, and $4/9f_n$, respectively. In Fig. 4(*a*), the waveform of the displacement has five bounces and five peaks every two revolutions. In Fig. 4(*b*), the rotational frequency, the larger

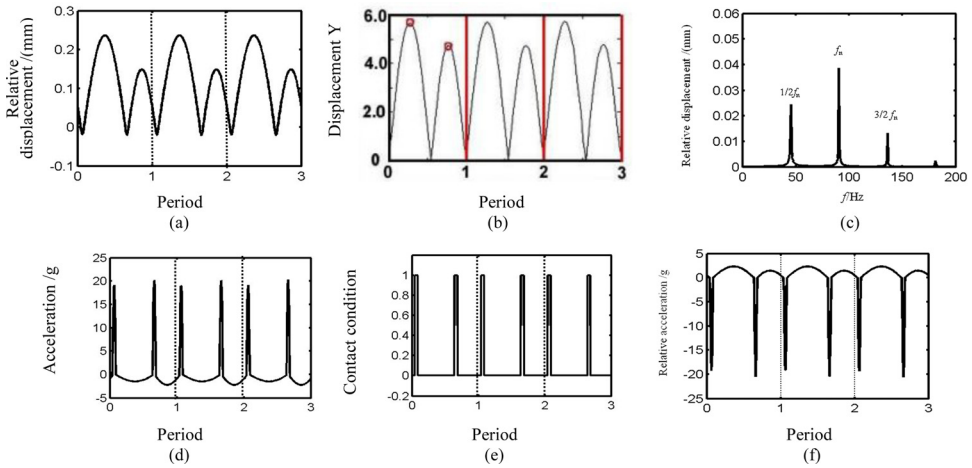

Fig. 2 Waveform characteristics at 1/2 times the natural frequency; (*a*) waveform, (*b*) waveform (the result of Literature [1]), (*c*) spectrum, (*d*) waveform, (*e*) waveform, and (*f*) waveform

asynchronous frequency, and the natural frequency of the system appear in the spectrum of the displacement. Figures 4(*c*) and 4(*d*) are from literature [1]. In Fig. 4(*e*), the changing period of stiffness is equivalent to twice the period of the rotational speed, so that 1/2× appears. In Fig. 4(*f*), the waveform of the acceleration of the rotor has five shocks every two rotations.

In Fig. 5(*a*), the waveform of the displacement has seven bounces and seven peaks every three revolutions. In Fig. 5(*b*), the rotational frequency, the larger asynchronous frequency, and the natural frequency of the relative displacement appear in the spectrum. Figures 5(*c*) and 5(*d*) are from literature [1]. In Fig. 5(*e*), the changing period of stiffness is equivalent to three times the period of the rotational speed, so that 1/3× appears. In Fig. 5(*f*), the waveform of the acceleration of the rotor has seven shocks every three rotations.

In Fig. 6(*a*), the waveform of the displacement has nine bounces and nine peaks every four revolutions. In Fig. 6(*b*), the rotational frequency, the stronger asynchronous frequency, and the natural frequency of the displacement appear in the spectrum. Figures 6(*c*) and 6(*d*) are from literature [1]. In Fig. 6(*e*), the changing period of stiffness is equivalent to four times the period of the rotational speed, so that 1/4× appears. In Fig. 6(*f*), the waveform of the acceleration of the rotor has nine shocks every four rotations.

As can be seen from Fig. 4 to 6, when the damping is not large enough and the rotational frequency is equal to $J/(2J+1)$, $(J+1)/(2J+1)$, and $(2J\text{-}1)/(2J)$ $(J=2, 3\ldots)$, the natural frequency of system, that is, the changing period of stiffness is equal to n times the period of the rotational speed, the rotational frequency, frequency division, and natural frequency will appear. Method of multiple scales was used to obtain the same results [9]; however, the relationship between the period of stiffness and the period of the rotational speed was not investigated. Literature [1] only provided the phenomenon of frequency division and frequency multiplication; however, the cause of this phenomenon was not explained.

The cascade plot of rotor acceleration at the subcritical speeds is shown in Fig. 7. The Campbell diagram from literature [1] is shown in Fig. 8. As can be seen from Fig. 7, the looseness fault characteristics are shown as the crossed streaks in the cascade plot, which are the asynchronous response frequencies. When the rotational frequencies are $1/4f_n$, $1/3f_n$, and $1/2f_n$, frequency multiplication will appear. When the rotational frequency is $2/3f_n$, 1/2× and the frequency multiplication will appear. When the rotational frequency is $3/4f_n$, 1/3×, 2/3× and the frequency multiplication will appear. Such similar phenomenon also appears at the transcritical and supercritical speeds. The quasi-period, bifurcation, and chaos will appear, when the rotational speed is not at the subcritical speeds of the paper described.

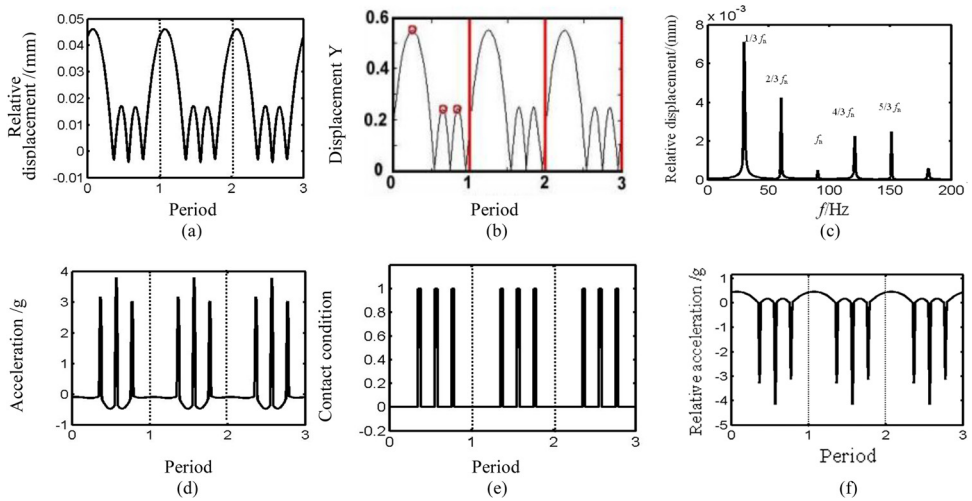

Fig. 3 Waveform characteristics at 1/3 times the natural frequency; (a) waveform, (*b*) waveform (the result of Literature [1]), (*c*) spectrum, (*d*) waveform, (*e*) waveform, and (*f*) waveform

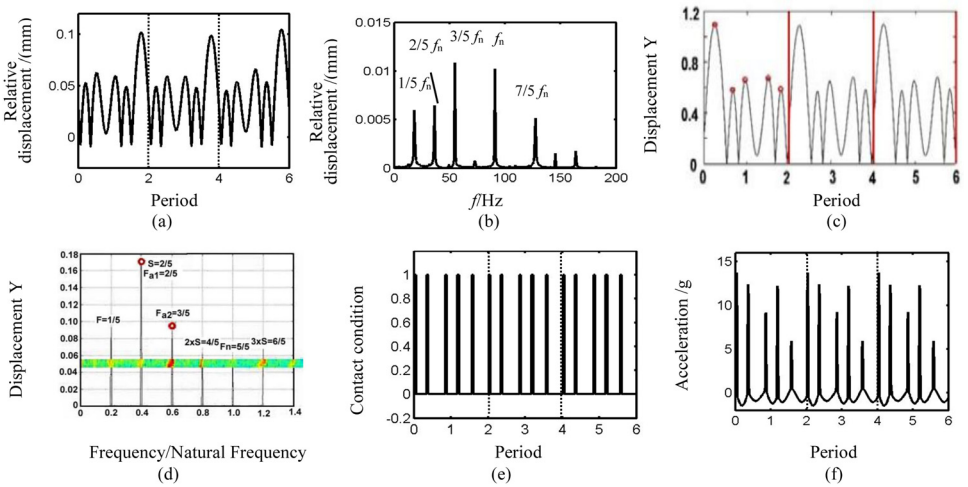

Fig. 4 Waveform characteristics at 2/5 times the natural frequency; (*a*) waveform, (*b*) spectrum, (*c*) waveform (the result of Literature [1]), (*d*) spectrum (the result of Literature [1]), (*e*) waveform, and (*f*) waveform

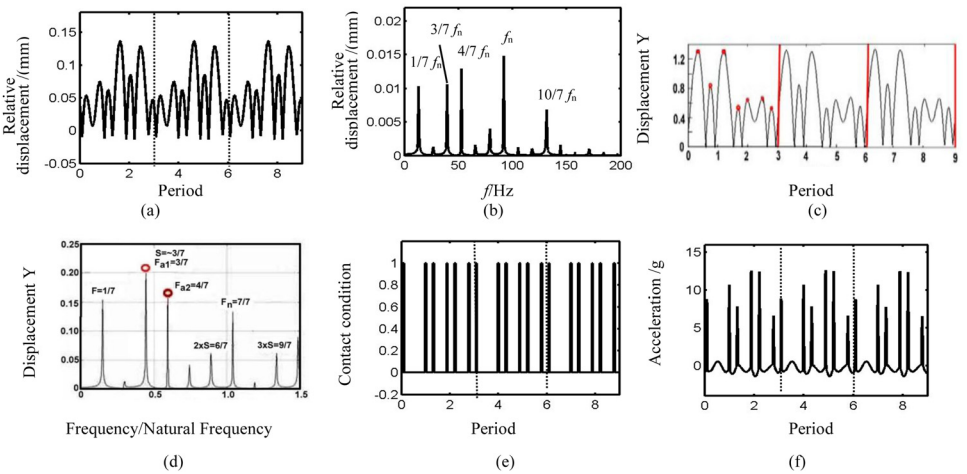

Fig. 5 Waveform characteristics at 3/7 times the natural frequency; (*a*) waveform, (*b*) spectrum, (*c*) waveform (the result of Literature [1]), (*d*) spectrum (the result of Literature [1]), (*e*) waveform, and (*f*) waveform

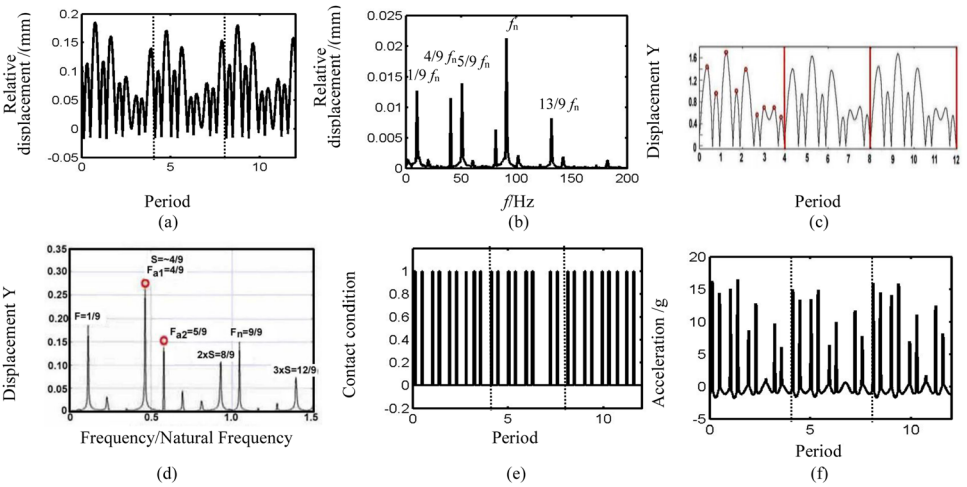

Fig. 6 Waveform characteristics at 4/9 times the natural frequency; (*a*) waveform, (*b*) spectrum, (*c*) waveform (the result of Literature [1]), (*d*) spectrum (the result of Literature [1]), (*e*) waveform, and (*f*) waveform

3 A Dynamic Model for Real Engine

3.1 The Structure Sketch Map for Real Engine. Rotor-bearing-Casing structure sketch map for real engine is shown in Fig. 9. The symbols in Fig. 9 are described as follows: the P_1 denotes fan disk, the P_2 denotes motor disk, the P_3 denotes compressor disk, the P_4 denotes the first turbine disk, the P_5 denotes the second turbine disk, the C_1 denotes the intermediate casing, the G_1 denotes the gear coupling between the fan shaft and the transmission shaft, the G_2 denotes the gear coupling between the transmission shaft and the compressor shaft, the G_3 denotes the gear coupling between the compressor shaft and the turbine shaft, the S_1 denotes the fan support bearings, the S_2 denotes the compressor front support bearings, S_3 denotes the compressor rear support bearings, S_4 denotes the turbine support bearings, the I_1 denotes the front installation node, the I_2 denotes the back installation node, k_g is the mesh stiffness of a gear pump, k_{f1}, k_{f2}, k_{f3}, and k_{f4} are the support stiffness between the rotor and the casing, k_c is the connection stiffness between the casing and the base, and T_1 is the compressor front measure point. In order to consider the strong nonlinearity caused by looseness fault, linear spring is adopted in support system (S_1, S_2, S_3, and S_4) without regard to the nonlinearity caused by rolling element.

3.2 Dynamic Model. The finite element model is used in the rotor models and the casing models. The rotors are coupled with other rotors and casings by forces and moments, its concrete modeling method is according to literature [15,17,18].

The rotor system's motion equation through the element's motion equations can be obtained, which is

$$(\mathbf{M}_s)\ddot{\mathbf{q}}_s + (\mathbf{C}_s - \omega\mathbf{G}_s)\dot{\mathbf{q}}_s + \mathbf{K}_s\mathbf{q}_s = \mathbf{Q}_s \tag{5}$$

where $\mathbf{Q}_s$ is the generalized external force vector, $\mathbf{M}_s$ is the mass matrix, $\mathbf{G}_s$ is gyroscopic matrix, $\mathbf{K}_s$ is the stiffness matrix of the system, and $\mathbf{C}_s$ is the damping matrix of the system.

In this paper, $\mathbf{C}_s$ is assumed to be proportional damping matrix, that is, $\mathbf{C}_s = \alpha_0\mathbf{M}_s + \alpha_1\mathbf{k}_s$, of which, α_0 and α_1 are constants. Because the ith order damping ratio is

$$\xi_i = \frac{1}{2}\left(\frac{\alpha_0}{\omega_i} + \alpha_1\omega_i\right) \tag{6}$$

Obviously, after any two natural frequencies and damping ratios of the rotor are acquired by modal experiment, α_0 and α_1 can be solved through Eq. (6), and the system's damping ratio matrix $\mathbf{C}_s$ can be obtained.

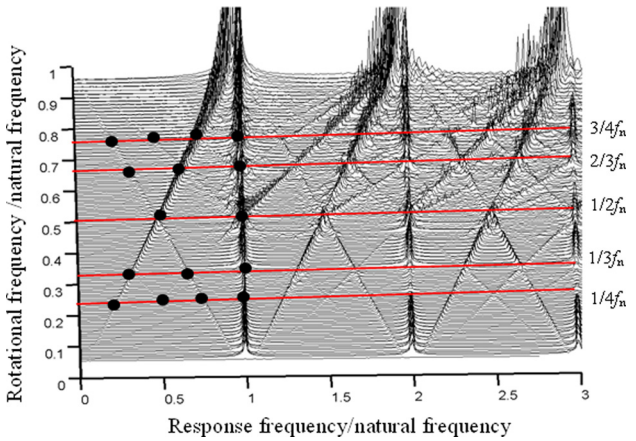

Fig. 7 Cascade plot showing under subcritical speeds

3.2.1 The Support Looseness Model. k_{f0} is assumed to be the equivalent stiffness between the rotor and the casing. Under the condition of relative displacement, piecewise linear between the rotor and the casing is considered in this paper, and the looseness fault model of a singe disk-rotor model is used in this paper. According to Eq. (3), the piecewise nonlinear stiffness k_f = can be expressed as

$$k_f = \begin{cases} k_{f0}/3 & (x_r - x_c > 0) \\ 20k_{f0} & (x_r - x_c < 0) \end{cases} \tag{7}$$

where x_r is the displacement of the rotor and x_c is the displacement of the casing. The looseness fault in horizontal is considered, and assuming that if the hard spring is contacted, the contact condition is marked 1, and if the soft spring is contacted, the contact condition is marked -1.

3.3 Solution of Finite Element Rotor-Casing Coupling Dynamic Model. Because the number of DOF in the finite element rotor-support-casing coupling dynamic model is very large, in addition, there are a lot of strong nonlinear factors, the implicit Newmark-β method is used to solve system's responses. This finite element rotor-casing coupling dynamic solution procedure is shown in Fig. 10.

4 Looseness Fault Analysis

4.1 Dynamic Model Parameters. The finite element parameters of the rotor and the casing can be found in Ref. [15] and the connection parameters of rotor-casing system are shown in Table 1. In this paper, $\alpha_0 = 5$, $\alpha_1 = 1.35 \times 10^{-5}$, elastic modulus is $E = 2.07 \times 10^{11}$ Pa, density is $\rho = 7.8 \times 10^3$ kg/m^3, and Poisson's ratio is $\mu = 0.3$.

4.2 Calculation Condition

(1) The looseness fault at the fan support in a horizontal direction is considered.
(2) The output is the casing horizontal vibration acceleration response in front of compressor fulcrum.
(3) The speed range is 15,000–70,000 rpm.

4.3 Critical Speed Analysis. Figure 11 shows the amplitude-speed curves of the casing lateral acceleration at the ninth node under imbalance fault. As can be seen from Fig. 11, the first-order, the second-order, and the third-order critical speeds are 26,400 rpm, 52,200 rpm, and 66,900 rpm, respectively.

4.4 Characteristics of Casing Acceleration at Different Speeds. Figure 12 shows cascade plot of the compressor rotor lateral displacement at the first node at different speeds. As can be seen from Fig. 12, when the rotational speed is around the first

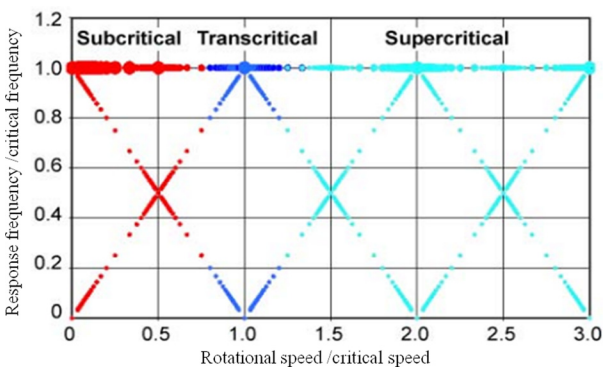

Fig. 8 Campbell diagram showing inferred generalized subcritical, transcritical, and supercritical response

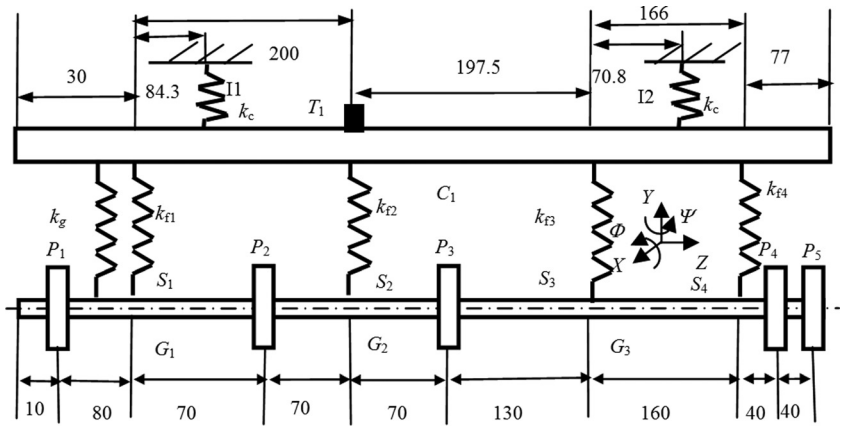

Fig. 9 Rotor-bearing-casing model sketch map of a type of real aeroengine (unit:mm)

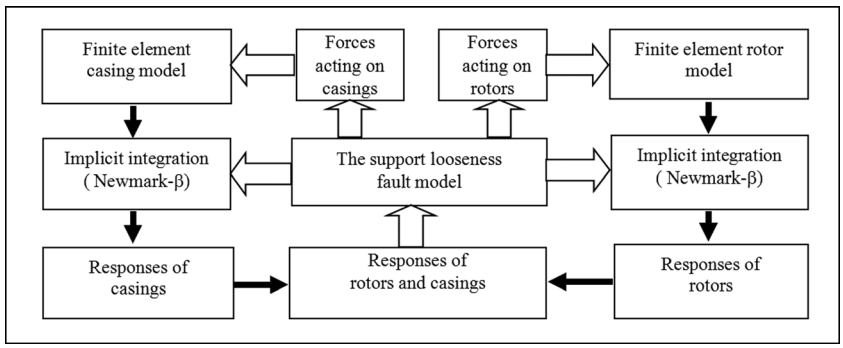

Fig. 10 Solving flow for rotor-casing coupling dynamics

three order critical speeds, that is 440 Hz, 920 Hz, and 1115 Hz, larger rotational frequency appears, meanwhile larger superharmonic resonance and subharmonic resonance appear. When the rotational speed is 17,400 rpm, which is 1/3 times the second-order critical speed, frequency multiplication appears and 3× is larger. When the rotational speed is 22,200 rpm, which is 1/3 times the third-order critical speed, frequency multiplication appears and 3× is larger. When the rotational speed is 27,600 rpm, which is 1/2 times the second-order critical speed, frequency multiplication appears and 2× is larger. When the rotational speed is 35,250 rpm, which is 5/4 times the first-order critical speed, frequency multiplication and 3/4× appear. When the rotational speed is 54,750 rpm, which is two times the first-order critical speed, frequency multiplication and 1/2× appear. When the rotational speed is 67,350 rpm, which is the third-order critical speed, frequency multiplication and 1/3× appear.

4.5 Characteristics of Asynchronous Vibration Response at Specific Rotational Speeds. In order to highlight the period components of rotational frequency, frequency multiplication, and frequency division in system, autocorrelation method is used to denoise the casing acceleration signal.

Figures 13–18 are the results of waveform characteristics that when the rotational speeds are 17,400 rpm, 22,200 rpm, 27,600 rpm, 35,250 rpm, 54,750 rpm, and 67,350 rpm, respectively. In Figs. 13(*a*)–13(*d*), the wave of the casing acceleration appears three shocks every rotation after the noise reduction of autocorrelation, and the larger 3× appears in spectrum after the noise reduction of autocorrelation; In Fig. 13(*e*), the waveform of

Table 1 Spring collection parameters of rotor casing

Collection	Node of rotor	Casing (node)	k_t (N/m)	c_t (N s/m)	k_f (N/m)	c_f (N s/m)
RC_1	3	2	1×10^8	2000	1×10^8	1000
RC_2	1	9	1×10^8	2000	1×10^8	1000
RC_3	11	16	1×10^8	2000	1×10^8	1000
RC_4	8	22	1×10^8	2000	1×10^8	1000
RK_1	6	4	1×10^8	0	1×10^8	0

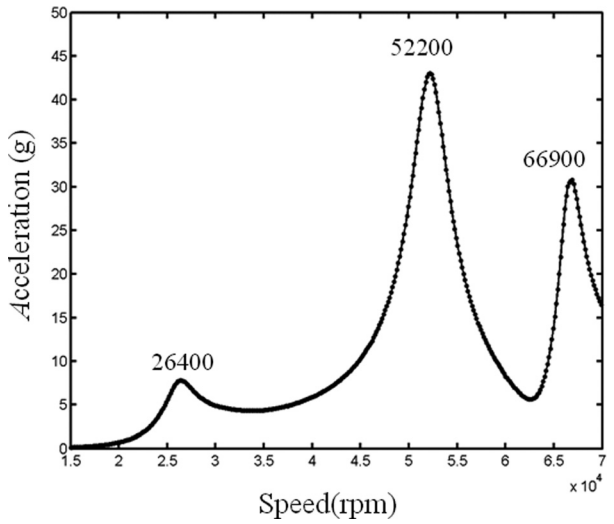

Fig. 11 Amplitude-speed curve of casing lateral acceleration (without looseness)

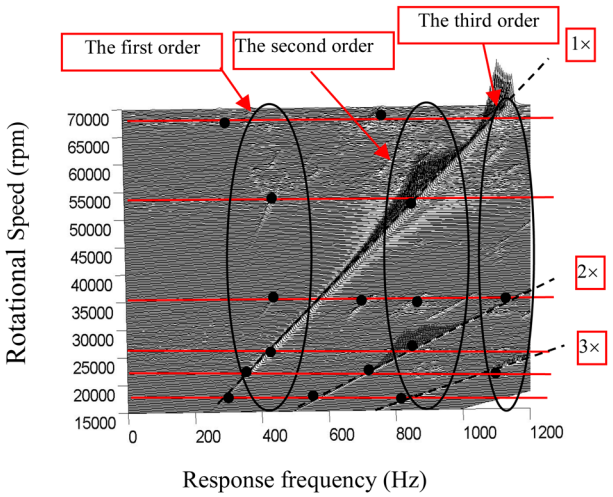

Fig. 12 Cascade plot of the casing acceleration response under 15,000–70,000 rpm

relative displacement has two bounces and two peaks every revolution, because the damping is larger in this model, the signal of displacement decays quickly, so the impact of displacement is not obvious. In Fig. 13(*f*), the stiffness changes one time every revolution, that is, the changing period of stiffness equals to the period of the rotational speed, and thus frequency multiplication appears.

In Figs. 14(*a*)–14(*d*), the wave of the casing acceleration appears three shocks every rotation after the noise reduction of autocorrelation, and rotational frequency, the larger 3× and asynchronous frequencies appear in spectrum after the noise reduction of autocorrelation. In Fig. 14(*e*), the waveform of relative displacement has two bounces and two peaks every revolution, because the damping is larger in this model, the signal of displacement decays quickly, so the impact of displacement is not obvious. In Fig. 14(*f*), the stiffness changes one time for every revolution, that is, the changing period of stiffness equals to the period of the rotational speed, and thus frequency multiplication appears.

In Figs. 15(*a*)–15(*d*), the wave of the casing acceleration appears two shocks every rotation after the noise reduction of

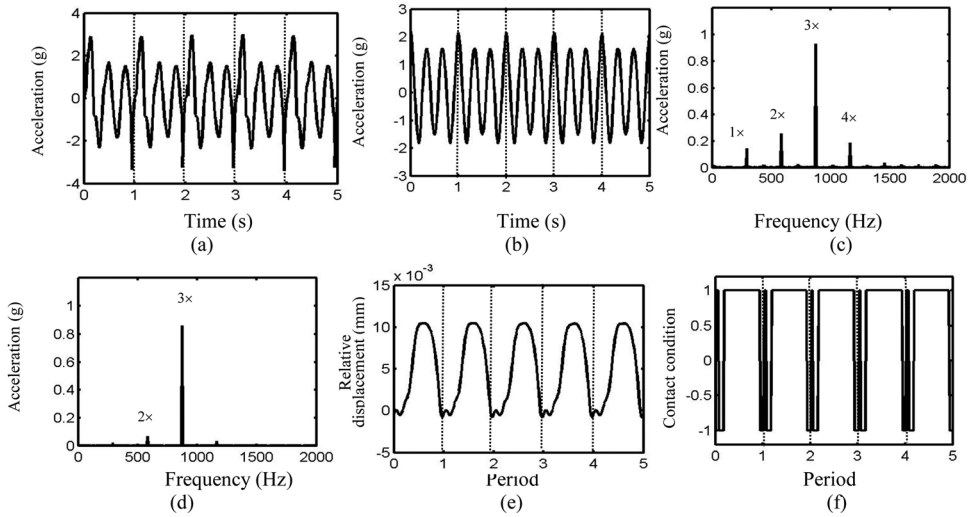

Fig. 13 The waveform characteristics at 1/3 times the second-order critical speed; (*a*) waveform before noise reduction, (*b*) waveform after noise reduction, (*c*) spectrum before noise reduction, (*d*) spectrum after noise reduction, (*e*) waveform, and (*f*) waveform

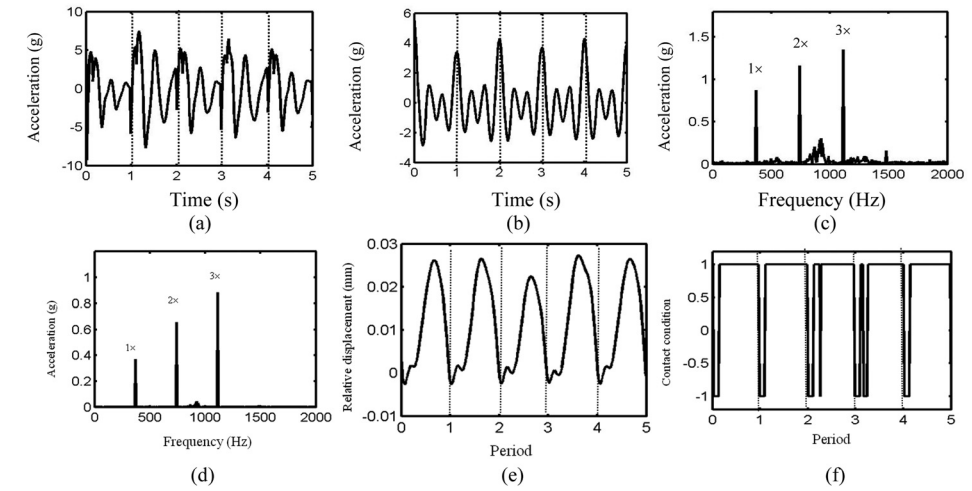

Fig. 14 The waveform characteristics at 1/3 times the third-order critical speed; (*a*) waveform before noise reduction, (*b*) waveform after noise reduction, (*c*) spectrum before noise reduction, (*d*) spectrum after noise reduction, (*e*) waveform, and (*f*) waveform

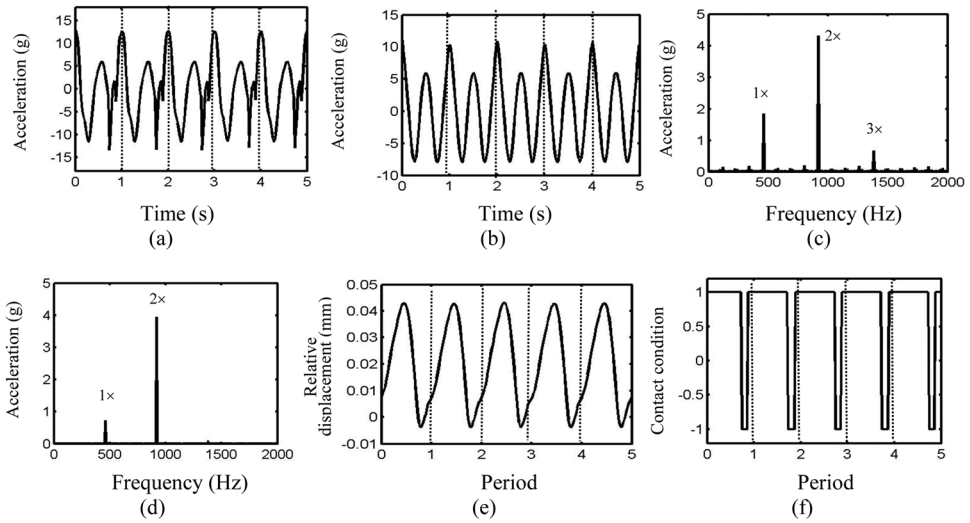

Fig. 15 The waveform characteristics at 1/2 times the second-order critical speed; (*a*) waveform before noise reduction, (*b*) waveform after noise reduction, (*c*) spectrum before noise reduction, (*d*) spectrum after noise reduction, (*e*) waveform, and (*f*) waveform

autocorrelation, and rotational frequency and the larger 2× appear in spectrum after the noise reduction of autocorrelation; In Fig. 15(*e*), the waveform of relative displacement has one bounce every revolution, because the damping is larger in this model, the signal of displacement decays quickly, so the impact of displacement is not obvious. In Fig. 15(*f*), the stiffness changes one time every revolution, that is, the changing period of stiffness equals to the period of the rotational speed, and thus frequency multiplication appears.

As can be seen from Figs. 13–15, when the changing period of stiffness equals to the period of the rotational speed, the pseudocritical superharmonic resonance appears, and the frequencies corresponding to the critical speeds will be excited. This phenomenon is in agreement with the experiments in literature [10].

In Figs. 16(*a*)–16(*d*), the wave of the casing acceleration appears five shocks every four rotations after the noise reduction of autocorrelation, and rotational frequency, frequency multiplication and asynchronous frequencies appear in spectrum after the noise reduction of autocorrelation. In Fig. 16(*e*), the waveform of relative displacement has three bounces every four revolutions, because the damping is larger in this model, the signal of displacement decays quickly, so the impact of displacement is not obvious. In Fig. 16(*f*), the stiffness changes three times every four revolutions, that is, the changing period of stiffness equals to four times the period of the rotational speed, and thus 1/4× appears.

In Figs. 17(*a*)–17(*d*), the wave of the casing acceleration appears two shocks every two rotations after the noise reduction of autocorrelation; the rotational frequency and 1/2× appear in spectrum after the noise reduction of autocorrelation, because 1/2× is weak, it is not obvious. In Fig. 17(*e*), the waveform of relative displacement has two bounces every two revolutions, because the damping is larger in this model, the signal of displacement decays quickly, so the impact of displacement is not obvious. In Fig. 17(*f*), the stiffness changes two times for every revolution, that is, the changing period of stiffness equals to two times the period of the rotational speed, and thus 1/2× appears.

In Figs. 18(*a*)–18(*d*), the wave of the casing acceleration appears three shocks for every three rotations after the noise reduction of autocorrelation; the rotational frequency, 1/3× and asynchronous frequencies appear in spectrum after the noise reduction of autocorrelation. In Fig. 18(*e*), the waveform of relative displacement has three bounces every three revolutions, because the damping is larger in this model, the signal of displacement decays quickly, so the impact of displacement is not

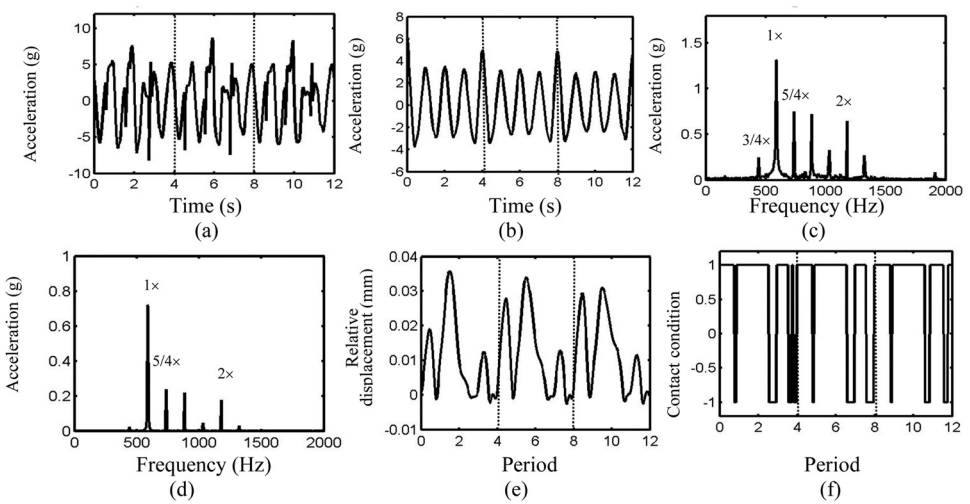

Fig. 16 The waveform characteristics at 5/4 times the first-order critical speed; (*a*) waveform before noise reduction, (*b*) waveform after noise reduction, (*c*) spectrum before noise reduction, (*d*) spectrum after noise reduction, (*e*) waveform, and (*f*) waveform

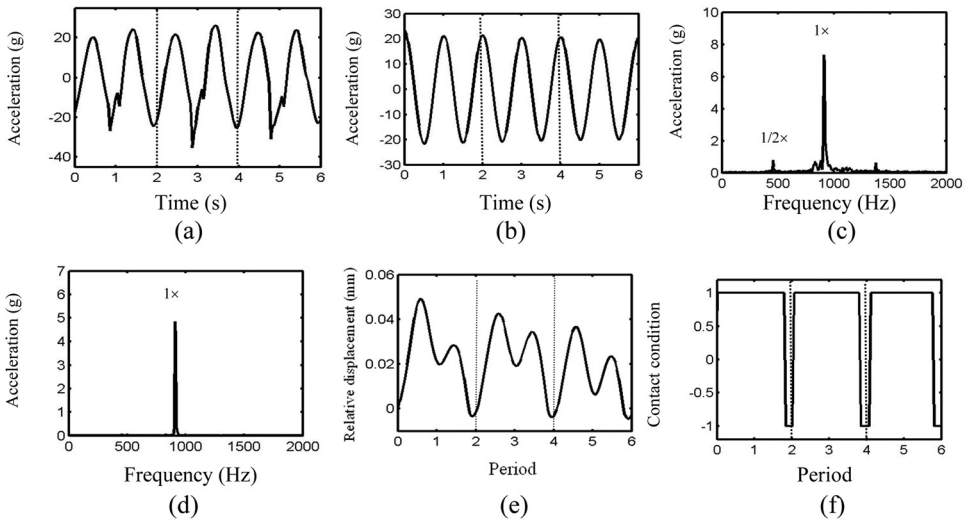

Fig. 17 The waveform characteristics at two times the first-order critical speed; (*a*) waveform before noise reduction, (*b*) waveform after noise reduction, (*c*) spectrum before noise reduction, (*d*) spectrum after noise reduction, (*e*) waveform, and (*f*) waveform

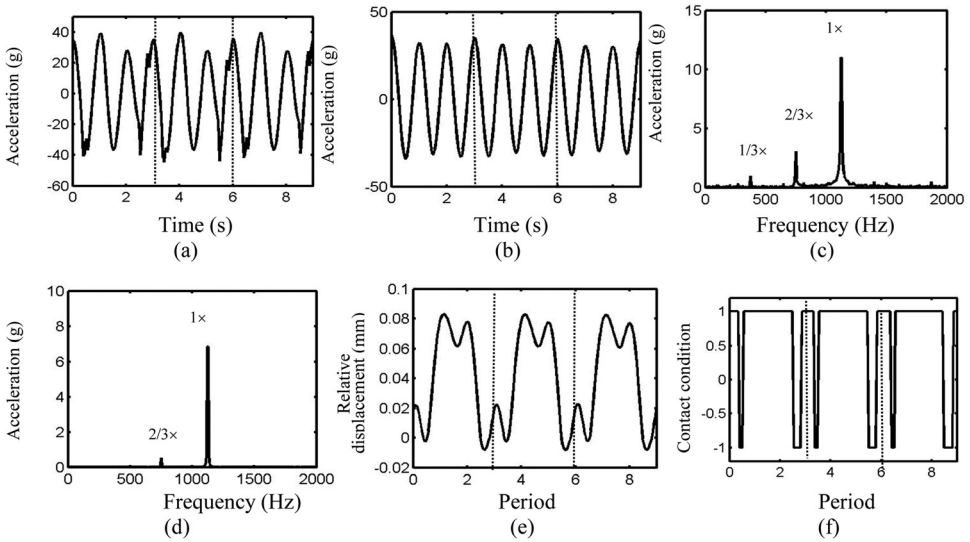

Fig. 18 The waveform characteristics at the third critical speed; (*a*) waveform before noise reduction, (*b*) waveform after noise reduction, (*c*) spectrum before noise reduction, (*d*) spectrum after noise reduction, (*e*) waveform, and (*f*) waveform

obvious. In Fig. 18(*f*), the stiffness changes two times for every three revolutions, that is, the changing period of stiffness equals to three times the period of the rotational speed, and thus $1/3\times$ appears.

As can be seen from Figs 16–18, when the changing period of stiffness equals to n times the period of the rotational speed, the pseudocritical subharmonic resonance appears, and the frequencies corresponding to the critical speeds will be excited. Method of multiple scales was applied to the differential equation of a single DOF, and the same results were obtained [9,10]; however, analytic solution of the differential equations of finite element cannot be obtained and the relationship between the changing period of stiffness and the changing period of the rotational speed was not investigated. Numerical calculation for the finite element model with looseness fault is of great significance.

5 Conclusion

In this paper, a single DOF lumped mass model with looseness fault and whole vibration model of real engine with looseness fault are established. Some results are obtained as follows:

(1) A single DOF lumped mass model with looseness fault is established, the asynchronous response characteristics are analyzed.
(2) Aiming at real engine, the dynamic model with the looseness fault is established. Numerical simulation method is used to obtain the engine casing acceleration response. It is found that the subharmonic resonance and superharmonic resonance will appear if the rotational speeds are equal to the fractional order critical speed and the critical speed. At specific rotational speeds, rotational frequency, frequency multiplication, and asynchronous frequency appear.
(3) A single disk-rotor model and certain type real engine whole vibration model with looseness fault were overall considered, and it is found that the pseudocritical subharmonic resonance and the pseudocritical ultraharmonic resonance are caused by the looseness fault. The reason leading to the asynchronous response characteristics is the relationship between the changing period of stiffness and the changing period of the rotational speed. When the changing period of stiffness is equivalent to the changing period of the rotational speed, frequency multiplication will appear

and the natural frequency will be excited at specific speeds. When the changing period of stiffness is equivalent to n times the changing period of the rotational speed, $1/n$ frequency division and frequency multiplication will appear and the natural frequency will be excited at specific speeds.

Acknowledgment

This work was supported by Funding of Jiangsu Innovation Program for Graduate Education KYLX_0295, the Fundamental Research Funds for the Central Universities and the NUAA Fundamental research funds, No. NS2013070.

References

[1] Ehrich, F. F., "A New Class of Asynchronous Rotor Dynamic Response in High-Speed Rotors," ASME Design Engineering Technical Conferences and Computers and Information in Engineering Conference, ASME Paper No. DETC2007-35912, pp. 1783–1788.
[2] Muszynska, A., and Goldman, P., 1995, "Chaotic Responses of Unbalanced Rotor Bearing Stator Systems With Looseness or Rubs," Chaos. Solitons Fractals, **5**(9), pp. 1683–1704.
[3] Yushu, C., and Shihai, L., 1986, "A Method for Finding the Sub/Super Harmonic Resonance Solution of Second Order Nonlinear Differential Equation and Its Application," Acta Mech. Sin., **18**(4), pp. 341–349 (in Chinese).
[4] Chu, F., and Tang, Y., 2001, "Stability and Non-Linear Responses of a Rotor-Bearing System With Pedestal Looseness," J. Sound Vibr., **241**(5), pp. 879–893.
[5] Guo, C., 2008, "Nonlinear Dynamic of Unbalance-looseness Coupling Faults of Rotor-ball Bearing-Stator Coupling System," J. Mech. Eng., **44**(3), pp. 82–88 (in Chinese).
[6] Goldman, P., and Muszynska, A., 1995, "Smoothing Technique for Rub or Looseness-Related Rotor Dynamic Problem," 15th ASME Biennial Vibration and Noise Conference, pp. 565–572.
[7] Lu, W., and Chu, F., 2009, "Experimental Investigation of Pedestal Looseness in a Rotor-Bearing System," Key Eng. Mater., **413–414**, pp. 599–605.
[8] Ji, Z., and Zu, J. W., 1998, "Method of Multiple Scales for Vibration Analysis of Rotor-Shaft Systems With Non-Linear Bearing Pedestal Model," J. Sound Vibr., **218**(2), pp. 293–305.
[9] Xin-liang, J., and Lan-Yue, L., 2003, "Superharmonic Resonance and Subharmonic Resonance of Nonlinear Structures Considering Nonsymmetrical Effect," Earthquake Eng. Eng. Vibr., **23**(5), pp. 50–56 (in Chinese).
[10] Anhua, C., and Jue, Z., 1997, "Theoretical Analysis and Experimental Research Into Super Harmonic Resonances of Rotor Systems," J. Cent. South Univ. Technol, **28**(3), pp. 270–273 (in Chinese).
[11] Lu, K., Jin, Y. L., Chen, Y. S., Cao, Q., and Zhang, Z., 2015, "Stability Analysis of Reduced Rotor Pedestal Looseness Fault Model," Nonlinear Dyn. (in press).
[12] Ma, H., Huang, J., Zhang, S., and Niu, H., 2013, "Nonlinear Vibration Characteristics of a Rotor System With Pedestal Looseness Fault Under Different Loading Conditions," J. Vibroeng., **15**(1), pp. 406–418.
[13] Behzad, M., and Asayeshthe, M., 2009, "Numerical and Experimental Investigation on Vibration of Rotors With Loose Disks," Proc. Inst. Mech. Eng., C: J. Mech. Eng. Sci., **224**(1), pp. 85–94.
[14] Ma, H., Zhao, X., Teng, Y., and Wen, B., 2011, "Analysis of Dynamic Characteristics for a Rotor System With Pedestal Looseness," Shock Vibr., **18**(1–2), pp. 13–27.
[15] Wang, H. F., and Chen, G., 2014, "Certain Type Turbofan Engine Whole Vibration Model With Support Looseness Fault and Casing Response Characteristics," Shock Vibr., **2014**, p. 683469.
[16] Zhai, W. M., 1996, "Two Simple Fast Integration Methods for Large-Scale Dynamic Problems in Engineering," Int. J. Numer. Methods Eng., **39**(24), pp. 4199–4214.
[17] Guo, C., 2012, "A Coupling Dynamic Model for Whole Aero-Engine Vibration and Its Verification," J. Aerosp. Power, **27**(2), pp. 242–254 (in Chinese).
[18] Aeroengine Design Manual Compiling Committee, 2000, *Aero-Engine Design Manual 19th Part: Rotor Dynamics and Whole-Engine Vibration*, Aviation Industry Press, Beijing, pp. 208–226 (in Chinese).